Nature of confining potentials in adatom-based quantum corrals and superlattices

Ahmed M. Othman [ORCID],[1] Mohammad A. Kher-Elden,[1] Ignacio Piquero-Zulaica [ORCID],[2] Johannes V. Barth,[2] Moukhtar A. Hassan,[1] Mohammed Farouk,[1] and Zakaria M. Abd El-Fattah [ORCID][1,*]

[1]*Physics Department, Faculty of Science, Al-Azhar University, Nasr City, E-11884 Cairo, Egypt*
[2]*Physics Department E20, Technical University of Munich, D-85748 Garching, Germany*

Quantum corrals represent an intriguing class of confining nanostructures engineered through tip manipulation of individual adsorbed species at surfaces and have contributed significantly towards our fundamental understanding of several quantum phenomena including quantum mirage and Kondo physics. Despite their maturity and ongoing research interest, the nature of adatom scattering/confining potentials including the question whether they represent potential barriers or wells remains elusive. Here we address this issue utilizing the electron plane-wave expansion and boundary element methods for several adatom-based quantum corrals and superlattices. We show that the experimentally reported modulation in the local density of states (LDOS) at the corral center can be equally well reproduced irrespective of the sign of adatom potential. The knowledge of the sign requires access to LDOS at/nearby adatoms, where bound states, so far undetected experimentally for corrals, should show up solely for negative adatom potential. Next we show that by arranging the adatoms into superlattices, the sign of the scattering potential can be undoubtedly identified without the quest for bound-state measurements. Our results agree with the experimentally fabricated Ce superlattice showing a clear signature of Ce adatoms acting as scattering potential wells. This unambiguous assignment of the potential sign is brought by the distinct band structures developed on coupling which lead into sign-dependent LDOS features. These findings are of fundamental and practical importance for the development of quantum designer artificial superlattices with tailored electronic structures.

I. INTRODUCTION

Shockley surface states [1] hosted at the (111)-terminated coinage metal surfaces represent model two-dimensional (2D) electronic systems with nearly free electron parabolic dispersion and featureless spatial local density of states (LDOS) [2–4]. They offer an ideal platform to explore several quantum phenomena when interacting with adsorbates [5–8], defects [9–14], predesigned nanostructures, and lateral superlattices [14–20] of various degrees of chemical composition, structural shape, and complexity, whereby radical transformation and modulation of the surface electronic structure and LDOS takes place. Surface-state electrons scattered off individual adatoms or molecules feature standing wave patterns experimentally accessible with scanning tunneling microscopy/spectroscopy (STM/STS), which can be used to probe the modulated surface electron dispersion [21] and to access the nature of the potential induced by the scattering centers.

While molecular scatterers are typically modeled as repulsive potential barriers [22], i.e., of positive sign with respect to the pristine metal surfaces, scattering at metal adatoms has shown to induce surface-state localization and the formation of bound states split off from the bottom of the surface state [23–25], indicative of adatoms acting as

potential wells [26]. Depending on the type of adatom, additional quantum phenomena, such as Kondo effect and magnetic exchange interactions can develop [27–30]. When several organic molecules are utilized to build confining and/or periodic nanostructures, the emerging modification of the electronic structures are often well understood as a simple scattering problem attributed to the repulsive finite potential barrier exerted by the molecules [22,31,32]. For recently explored metal-organic nanoporous networks, however, heterogeneous potential landscapes are proposed, where contradicting studies consider the potential at coordinating adatoms as attractive [33,34] or repulsive [35–37]. Notably, in the pioneering work of Crommie *et al.* [5], Fe adatoms were arranged into quantum corrals via STM tip manipulation, where well-defined confined states, showing up as sharp peaks in the conductance spectra were measured at the corral center. While a simple particle-in-a-box model with an impenetrable hard-wall barrier could qualitatively explain the data, the finite LDOS linewidth reflects a leaky semitransparent barrier. This broadening effect together with the possible absorption at adatoms due to inelastic scattering into bulk states, were later reproduced making use of the multiple scattering approach [6].

The lack of conclusive experimental evidence for bound states at the corral barriers renders the sign of the adatom scattering potential in these nanostructures yet unidentified. Likewise, adatom-based superlattices, such as the Ce/Ag(111) hexagonal superlattice self-assembled at low temperature due

---

*Corresponding author: z.m.abdelfattah@azhar.edu.eg

to surface-state mediated organization, stands as a model system to unveil the sign of the adatom potential [19,38–40]. However, even though the scattering electronic states of the system could be well reproduced using a simple tight-binding (TB) model, in which the model predicted a bound state below the surface-state onset, this could not be clearly identified experimentally. The mismatch between the 2D TB LDOS above the bound-state energy and experimental dI/dV map, specifically at the adatom positions, was attributed to large tip-adatom distance and possible leakage of the bound state into the bulk, although faint intensity at adatom positions has been later detected for a slightly larger Ce superlattice [39]. Therefore, unlike single adatoms, for adatom-based quantum corrals and nanostructures, there is no concrete evidence to whether adatoms act as quantum wells or barriers, and a rigorous identification of bound states is experimentally lacking. In fact, even though the distinct phase shift for typical standing wave patterns inside closed nanostructures could also be utilized to unravel the potential sign, this effect may be screened during measurements with a slight STM tip drift and/or image distortion as we show later. Likewise, a high density of on-surface adatoms should lead to a noticeable shift of the surface-state band, thereby unraveling the potential sign, when measured by angle-resolved photoemission spectroscopy (ARPES), but this space-averaging technique is not suitable for finite nanostructures, as it demands the assembly of a macroscopically ordered high density of adsorbates on the surface.

Here we address this ambiguity of the potential sign in adatom-based quantum corrals and superlattices using electron plane-wave expansion (EPWE) and boundary element method (EBEM) [33,41–43]. We show that the experimentally measured LDOS at the corral center cannot be used to unveil the sign of the confining potential. The knowledge of the latter requires precise and practically challenging LDOS measurements at/near the position of adatoms, where a bound state below the onset of the surface state should arise solely for attractive adatom potentials. Next, we demonstrate that the sign of the scattering potential can be unveiled when adatoms are arranged into superlattices, where the potential sign can be revealed by measuring LDOS away from adatom positions and without the need of identifying any signature of bound states. Comparing our simulations with the well-known Ce superlattices self-assembled on Ag(111), we unambiguously conclude that the scattering potential associated with Ce adatoms is attractive. We also demonstrate the applicability of our EBEM approach here followed to reproduce the bound-state features measured for individual adatoms on metallic substrates. The knowledge of the potential sign here addressed is decisive for the fundamental understanding of quantum confinement and scattering, as well as for the fabrication of adatom-based nanostructures and superlattices with on-demand electronic properties.

II. THEORETICAL METHODS

We simulate the electronic properties of adatom-based quantum corrals and superlattices by solving the one-electron Schrödinger equation for a 2D surface potential $V_s(\mathbf{R} = (x, y))$ where adatoms are defined as circles filled with muffin tin potential (V) on top of a homogeneous metal substrate of constant potential (V_0), as sketched in Fig. 1 and Fig. 2. We then solve, for the energies E and wave functions $\psi(\mathbf{R})$, the Schrödinger equation,

$$-\frac{\hbar^2}{2m_{\text{eff}}}\nabla^2\psi(\mathbf{R}) + V_s(\mathbf{R})\psi(\mathbf{R}) = E\psi(\mathbf{R}), \quad (1)$$

following two different methods, namely the EBEM and the EPWE, detailed in Refs. [33,41,42]. The energy is referenced to the surface-state onset of the pristine metal substrate [i.e., -435 ± 15 meV and -65 ± 10 meV for Cu(111) and Ag(111), respectively], and the effective mass m_{eff} is changed in the range 0.35 to 0.45 m_e for comparison with experimental data.

For single adatoms, quantum corrals, resonators, and stadiums we solve Eq. (1) for the energy- and spatial-dependent LDOS using EBEM. For the superlattice periodic systems EPWE is used to calculate the band structure, LDOS, and the photoemission intensity following the equations in Ref. [41]. A finite number of reciprocal lattice vectors within a sufficiently large distance $g_{\text{max}} = 10$ to the origin in reciprocal space is used for decent convergence, corresponding to ~100 plane waves. For all the systems explored we add a Gaussian broadening of 15 meV. The here-employed 2D EPWE/EBEM method has proven successful in modeling electron scattering and confinement in a variety of systems, including metallic and organic/metal-organic networks, single molecules, polymers, graphene, graphene-based nanostructures, and other 2D materials [20,22,41,46,47]. The combined EPWE/EBEM package used in this work is developed by Prof. F. Javier García de Abajo.

III. RESULTS AND DISCUSSION

Figure 1 presents the EBEM surface potential and simulated LDOS for selected Fe adatom-based quantum corrals compared to experimental data and multiple scattering (MS) theory. In Fig. 1(a), the potential landscape defining a quantum corral made of 48 Fe adatoms (radius $R = 71.3$ Å) is depicted, whereby the gray background represents the Cu(111) substrate with potential $V_0 = 0$ and red circles (radius $r = 3$ Å) denote the muffin tin Fe adatom potentials acting either as quantum wells ($V = -0.55$ eV) or barriers ($V = +0.55$ eV). The reference energy is chosen to be -435 ± 10 meV, corresponding to the onset of Cu(111) surface state [5,23], while the effective mass (m_{eff}) is set to $(0.41 \pm 0.01)m_e$ and $(0.36 \pm 0.01)m_e$ for negative and positive Fe potentials, respectively. We note that for positive adatom potential $m_{\text{eff}} = (0.36 \pm 0.01)m_e$, i.e., smaller than the one of pristine Cu(111), is required to best fit the experimental dI/dV curves (see Fig. S1 in the supplemental material (SM) [48]), which could indicate that Fe scatterers are not repulsive. However, this is not conclusive since for several systems with on-surface adsorbates or dopants, effective mass renormalization has been recurrently observed [22,49,50]. Furthermore, the potential landscapes defined in this work are 2D and, therefore, correspond to the lateral electron confinement in ultrathin materials such as monolayer or bilayer systems where bulk contributions are minimal. However, for metallic thin films or substrates the coupling to
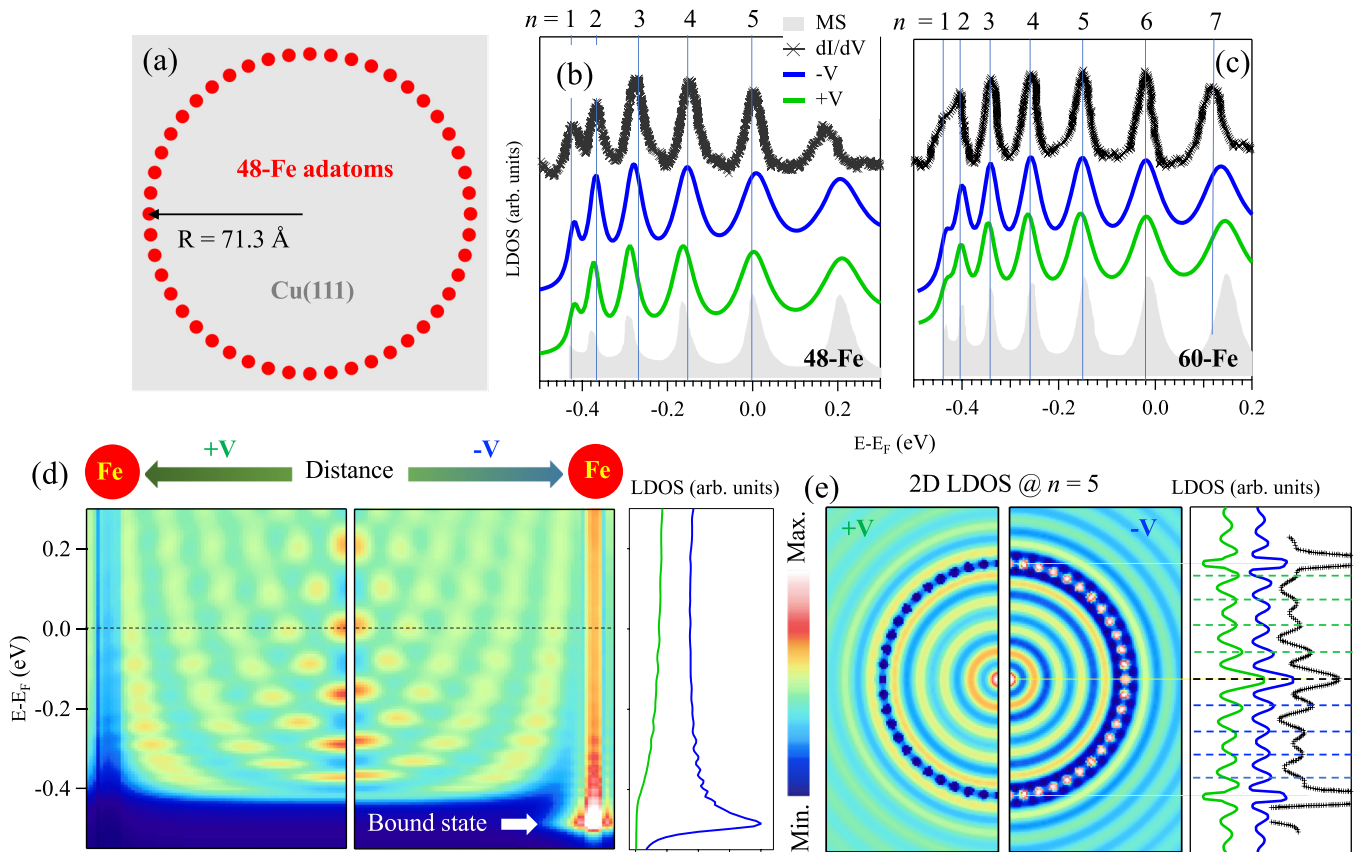
FIG. 1. EBEM vs. dI/dV for selected Fe-based quantum corrals. (a) The potential landscape for a quantum corral made of 48 Fe adatoms (red) on top of the Cu(111) substrate (gray). The corral and Fe adatom radii amount to $R = 71.3$ Å and $r = 3$ Å, respectively. Positive and negative potentials ($V = \pm 0.55$ eV) with respect to the Cu substrate ($V_0 = 0$) are assigned to Fe adatoms. [(b) and (c)] Experimental dI/dV spectra (black), multiple scattering (MS) (gray), and EBEM (blue and green) calculated LDOS taken at the center of quantum corrals made of 48 (b) and 60 (c) Fe adatoms. EBEM LDOS spectra correspond to positive (green) and negative (blue) potentials. The experimental data and MS curves are taken from Refs. [5–7,44,45]. The vertical lines denote the energetic positions of the confined states. (d) Calculated linescan over the diameter for the 48-Fe-adatom circular corral for positive $+V$ (left) and negative $-V$ (right) potentials, where the white arrow marks the bound-state position. The LDOS spectra taken at the position of Fe adatoms are shown on the right for the two potentials. (e) EBEM calculated 2D LDOS maps at the Fermi energy (i.e., at $n = 5$ state) for the 48-Fe ring, considering positive (left) and negative (right) potentials at adatoms. Line profiles (blue and green) taken from the corral center passing through Fe adatom, displayed on the right, show the intensity protrusion (depression) for negative (positive) Fe potential, compared to the experimental data (black). Dashed lines denote the position and number of antinodes inside the corral.

bulk states can be approximately modeled within the EBEM approach by utilizing a complex potential with an appropriate imaginary component to account for the strength of such coupling, as we discuss later. The EBEM simulated LDOS spectra at the corral center for negative (blue) and positive (green) adatom potentials are depicted in Fig. 1(b). The two spectra are practically identical, both featuring multiple confinement peaks ($n = 1$–6) of finite width, and reasonably agree with the experimental dI/dV (black) and earlier MS LDOS simulations (gray) as adapted from Refs. [5–7,44,45]. It is worth noting that, in recent years, this quantization of electron gas inside smaller CO-based quantum corrals stimulated the consideration of these confining structures as artificial atoms, where the characteristic orbital shape of each individual peak (i.e., energy level) could be compared to atomic s, p, and d orbitals, and they can additionally be coupled to emulate molecules and artificial lattices [51,52]. A similar level of matching is obtained for other Fe adatom-based nanostructures, such as the larger 60 Fe adatom (radius $R = 88.7$ Å)

circular corral [Fig. 1(c)] and for the quantum stadium made of 76 Fe adatom (see Fig. S2 of the SM [48]). In fact, we can still reproduce the experimental data and previous MS simulations, utilizing stronger positive or negative potentials (see Figs. S3 and S4 of the SM [48]), indicating that not only the sign but also the absolute value of the potential cannot be determined solely from LDOS measurements at the corral center. This ambiguity can be extended to adatom-based open nanostructures, such as quantum resonators made of Cu, Ag, or Co adatoms on (111)-oriented metallic substrates [53,54], whereby the LDOS features measured at the center or outside the resonator can be practically reproduced by both positive or negative potentials (see Fig. S5 of the SM [48]).

To search for possible electronic differences between attractive and repulsive adatom potentials, we performed LDOS energy-dependent spatial line scan simulations, starting from the center of the corral towards the Fe-adatom position, as shown in Fig. 1(d) for positive (left) and negative (right) adatoms potentials. The two scans are practically mirror
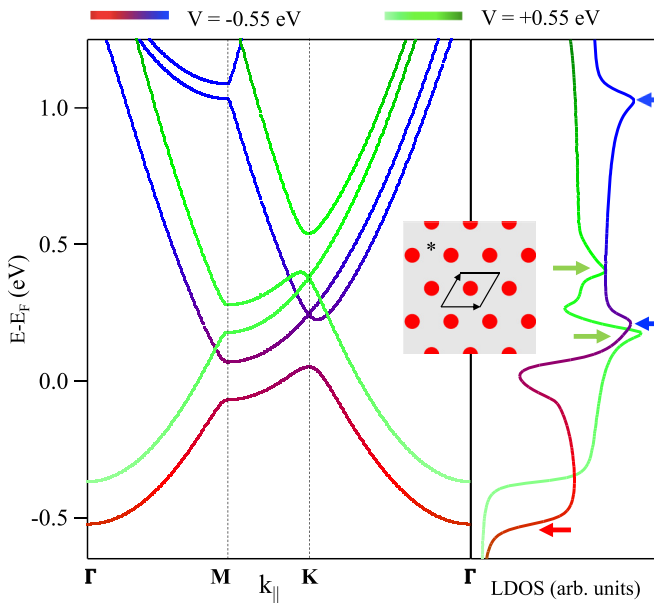
FIG. 2. Electronic structure of adatom-based hexagonal superlattices. The band structure along ΓM$K$$\Gamma$ directions for a hexagonal Fe superlattice of periodicity $a = 15.4$ Å for positive (green) and negative (red-blue) adatom potential. The unit cell (black arrows) and potential landscape are shown in the inset. On the right, the corresponding LDOS taken at the substrate position indicated by an asterisk in the inset is presented. The red arrow points to the bound-state onset, while green and blue arrows define LDOS features for positive and negative potentials, respectively.

images, except at/near adatom position, where a bound state is developed solely for adatom quantum wells (white arrow). LDOS profiles (green and blue) taken at the adatom positions show a clear bound-state peak at ~ -0.49 eV (blue) for negative adatom potential, similarly to states reported for single adatoms on Cu(111) and Ag(111) [23–25,55]. For closed multiple-adatom quantum corrals and stadiums, as well open adatom resonators, so far no evidence of bound states below the onset of the surface state has been reported and/or measured [5,6,54]. In Fig. 1(e) we present 2D LDOS maps for positive (left) and negative (right) potentials taken at the Fermi energy (i.e., corresponding to $n = 5$ state for the 48-Fe ring), both enclosing standing wave patterns featuring five antinodes resulting from interference due to the scattering of the two-dimensional electron gas by adatoms at the corral barrier. The obvious distinction occurs at adatom positions, where they appear as intensity depressions (protrusions) for positive (negative) potentials. The period of oscillation is comparable for both repulsive/attractive potentials and the experiment (see line cuts in Fig. 1(e) across the corral) with a wavelength, measured from the central intensity, of 15.5 ± 0.05 Å corresponding to half the Fermi wavelength of the Cu(111) Shockley surface state [2]. Dashed lines positioned at the antinodes highlight the phase relation between the standing wave patterns at the interior of the corral for positive (green) and negative (blue) potentials. A clear phase shift which is progressively increasing from the corral center towards the adatoms is noted, thereby carrying information about the potential sign as demonstrated, e.g., for

adsorbate-adsorbate interactions mediated by surface electrons [56,57]. Comparing these theoretical phases with the experimental line cut (black) for the 48-Fe adatom corral we notice that the two theoretical phases can fit the experiment, possibly due to STM tip drift and/or image distortion in the experimental data, rendering the identification of the potential sign challenging. The thorough analysis presented in Fig. 1 makes it clear that a conclusive evidence of the presence or absence of bound states is required to unravel the potential sign of adatoms. Indeed, LDOS measurements at adatoms can be largely convoluted with topography, leading to intensity protrusions at adatoms artificially resembling bound states. Likewise, the bound state, if present, is possibly leaking into bulk states and forming a dispersive band with weak/broad LDOS features. These combined effects potentially suppress notable tunneling signals from adatoms, thereby rendering the identification of the potential sign in quantum corrals, and similar adatom-based finite nanostructures, rather challenging.

Next, we show that by arranging the adatoms into superlattices, contrary to fully enclosed confining nanostructures such as corrals, the scattering solutions of the electronic structure are quite distinct for positive and negative adatom potentials. Figure 2 depicts the potential landscape (see inset) for a hexagonal superlattice made of Fe adatoms (red) on Cu(111) (gray) with a periodicity of 15.4 Å. This lattice parameter is chosen to coincide with half the Fermi wavelength of Cu(111) surface state where the self-assembly could be mediated by surface electrons [58], although different lattice spacing can be achieved by STM tip-manipulation protocols [19,22,34,39]. The EPWE calculated band structures along high symmetry ΓM$K$$\Gamma$ directions for positive (green) and negative (blue-red) adatom potentials are shown in Fig. 2 (left). The prominent differences are the energetic down-shift and the opening of a large K-point gap for negative potential adatoms, in contrast to the upward shift and Dirac-like dispersion obtained from adatom quantum barriers. These band structures are originated from the distinct confinement of surface electrons by adatoms of different potential sign. For a positive adatom potential, surface electrons are confined into a honeycomb artificial atom pathway resulting in a graphenelike band structure [59]. In contrast, for a hexagonal lattice of attractive adatom potential, the artificial atom sites are located under/around the adatoms resulting in coupled artificial atoms analogous to hexagonal quantum dots routinely utilized, for example, in metal-organic porous networks [22]. When LDOS is simulated at the substrate position indicated by an asterisk in the inset, i.e., at the center of the triangle formed by 3 Fe adatoms, the spectra contain distinct features (Fig. 2, right) carrying information about the sign of the scattering potential. For negative adatom potential, an edgelike feature below the surface-state onset (see red arrow) shows up at ~ -0.524 eV corresponding to the bound-state band. This feature is ~ 0.156 eV lower in energy than the scattered surface-state LDOS edge for positive adatom potential. Furthermore, close to the Fermi energy, the LDOS spectra exhibit either single or double peaks (see arrows), which could be distinguished in STS experiments. On the energy scale of the presented graph, an additional high energy peak at ~ 1.03 eV (blue arrow) is present, for negative adatom
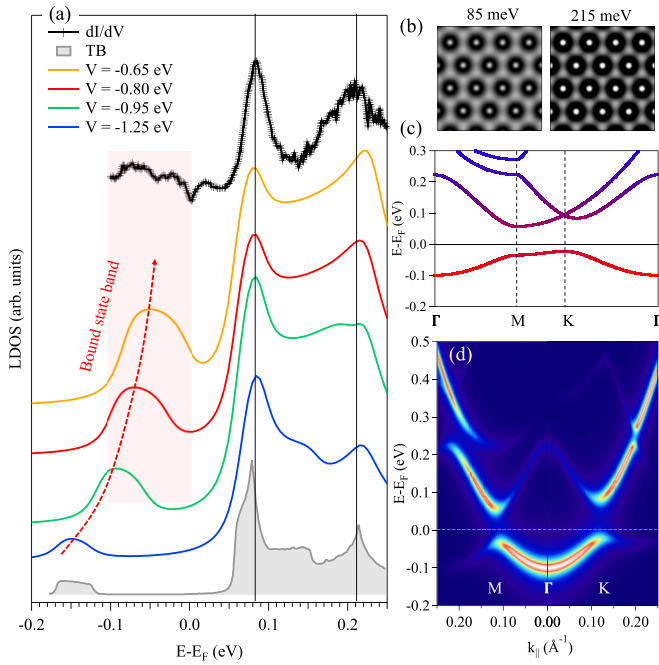
FIG. 3. Electronic properties of a self-assembled Ce hexagonal superlattice on Ag(111). (a) Experimental dI/dV curve (black) measured at the center of a triangle formed by three Ce adatoms and the corresponding simulated TB LDOS (gray) taken from Refs. [38,39]. The LDOS here simulated by EPWE are shown as colored curves for different adatom potentials. The shaded red area marks a possible experimental bound-state feature, and the red arrow shows the shift of the bound-state band with varying adatom potential. (b) Two-dimensional LDOS maps simulated using EPWE at the energies 0.08 and 0.215 eV. (c) The band structure along ΓMKΓ directions for Ce adatom potential of -0.8 eV. (d) The corresponding photoemission intensity simulation along ΓM (left) and ΓK (right) directions.

potential, which originates from bands at the second energy gap in the corresponding band structure. Although the energetic position of this peak is strongly periodicity dependent (see Fig. S6 of the SM [48]), the comparative LDOS here calculated away from adatom positions, conclusively defines the potential sign. In this context, the LDOS experimentally measured for molecular graphene designed by STM tip manipulation of CO molecules on Cu(111) substrate, obviously results from positive CO potential barriers [59]. Likewise, a square arrangement of adatoms (see Fig. S7 of the SM [48]) also leads to distinct electronic properties for positive and negative potentials, as demonstrated for CO-based square and Lieb lattices [60].

Following previous discussions, we proceed to compare our simulations with the first reported Ce adatoms hexagonal superlattice, fabricated by surface-state-mediated self-assembly on Ag(111) [19,38–40]. In Fig. 3(a), the experimental dI/dV curve (black) and the corresponding TB LDOS (gray) at the center of Ce triangle (see asterisk in Fig. 2) for hexagonal Ce-based superlattice of periodicity 32 Å as obtained from Refs. [38,39] are presented. The TB LDOS nicely fits the two experimental LDOS peaks at 0.083 and 0.215 eV, with an additional weak broad band below -0.1 eV (corresponding to a bound-state band) shows up in TB

calculations and not measured experimentally. Our EPWE LDOS simulations nicely reproduce the experimental dI/dV for different absolute values of negative adatom potential and also for several hexagonal Ce superlattices of different periodicities (see Fig. S8 of the SM [48]). In contrast, by treating Ce adatoms as repulsive scatterers, i.e., positive potential barriers, for any combination of potential and effective mass, it was not possible to match the experimental data (see Fig. S9 of the SM [48]). Therefore, it is unambiguously concluded that Ce adatoms in this superlattice act as potential wells. However, the determination of the absolute value (i.e., strength) of this negative potential requires the identification of bound-state features. By changing the adatom potential from -0.65 to -1.25 eV and m_{eff} from 0.41 to 0.46 m_e, respectively, the bound-state broad feature below the Fermi energy systematically shifts towards higher binding energy approaching the TB band at the highest absolute value of the potential. Indeed, the experimental dI/dV data contains some features below the Fermi energy (see shaded red area) that could be assigned to a bound-state matching for a -0.8 eV scattering barrier. By performing simulations for 2D LDOS maps at the energy of the two peaks, Fig. 3(b), we see that the probability density is localized at the substrate in a honeycomb path as well as at adatoms positions. While this is consistent with TB results, the experimental dI/dV maps reproduce the honeycomb intensity at substrate but reveal no intensity at adatoms [38]. This can be likely attributed to large tip-Ce distances and/or to the leakage of bound states into the bulk. The band structure of such Ce superlattice, for $V = -0.8$ eV depicted in Fig. 3(c), agrees with the TB model consisting of a Fermi gap which electronically stabilizes the surface-state mediated growth. Below the Fermi energy, a bound-state band (red) is present, while the scattering states at the upper/lower edges of the first/second energy gaps are responsible for the two LDOS peaks observed in Fig. 3(a). By simulating the angular dependence of the photoemission intensity, Fig. 3(d), the occupied states consist of a parabolic bound-state dispersion shifted to higher binding energy compared to the pristine Ag(111) Shockley surface states [2]. This shift together with the Fermi gap could be probed with ARPES, although the Ce superlattice is only stable at $T < 4$ K. Indeed, for metal-organic networks containing a stable arrangement of Co and Cu adatoms into honeycomb and kagome superlattices on Au(111) and Cu(111), respectively, ARPES measurements revealed downward shifts below the surface-state onset of the metallic substrate, consistent with negative adatom potentials and agreeing with DFT predictions [22,36,37].

While the sign of the adatom potential could be revealed by contrasting the electronic features in superlattices formed by an array of quantum barriers or wells, the absolute value of the negative potential, as discussed, demands clear measurement of the bound states. These are recurrently measured for individual adatoms on metal substrates [23–25]. Below we give an estimate of the magnitude of negative adatom potentials for reported adatom/substrate systems hosting bound states. In Fig. 4(a) we present the optimal Newns-Anderson model fit to the experimental dI/dV curves measured at the center of single Co and Cu adatom deposited on Cu(111) labeled by the green and blue symbols, respectively, and taken from Refs. [24,25]. The energy axis is referenced to the onset of
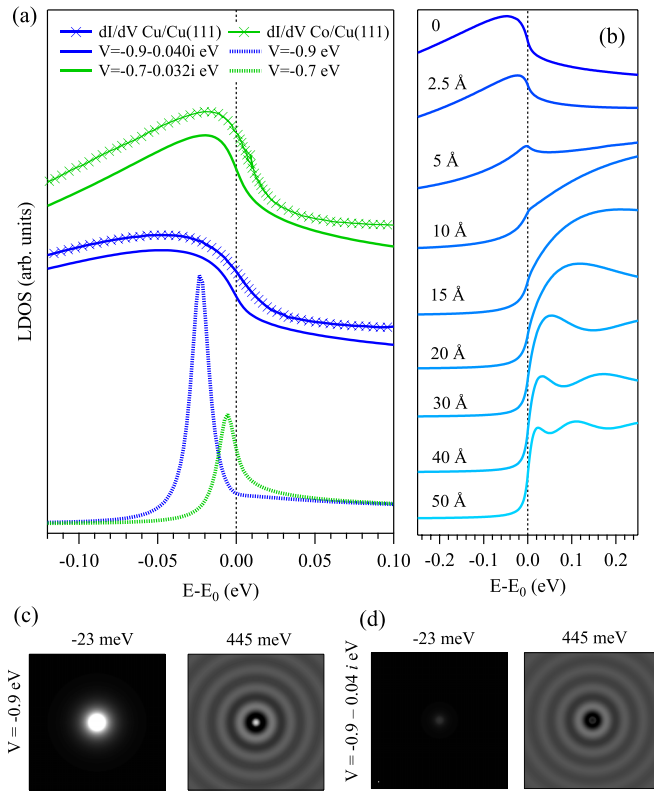
FIG. 4. Bound state of individual adatoms on metallic substrates. (a) EBEM simulated LDOS at the center of single Co (green) and Cu (blue) adatoms on Cu(111) substrate compared to the Newns-Anderson model fit to the experimental dI/dV spectra (symbols) taken from Refs. [24,25]. Dashed and solid curves correspond to LDOS for real and imaginary adatoms potentials, respectively. (b) EBEM simulated LDOS at different positions from the adatom center (0) up to 50 Å away. The bound-state LDOS feature transforms into surface-state edgelike ~10 Å away from the adatom. [(c) and (d)] Two-dimensional LDOS maps simulated at the bound state (-23 meV) and Fermi (445 meV) energies for real (c) and imaginary (d) adatom potentials.

the Cu(111) surface state, being $E_0 = -0.445$ eV. The curves exhibit a bound-state feature distinct from the typical surface-state edge, and they appear as broad intensity shoulders right below the surface-state onset with different energetic position and width for Co and Cu adatoms. We construct an EBEM potential landscape consisting of a single circular muffin tin potential V representing the adatom on Cu(111) substrate. For Co/Cu(111) and Cu/Cu(111) systems we set $V = -0.7$ eV and $V = -0.9$ eV, respectively, and $m_{eff} = 0.41\, m_e$. The simulated LDOS curves (dashed) at the center of Co (green) and Cu (blue) adatoms exhibit a sharp peak slightly below the surface-state onset ($E - E_0 = 0$), where their spectral shape is clearly not consistent with the dI/dV curves. However, the matching with the experiment can be achieved simply by adding an imaginary component to the adatom potential to account for possible losses due to coupling with bulk bands. The imaginary part of the potential allows the attenuation of states with Fourier components of probability density at the bulk projected bands of Cu(111) for individual or multiple adatom systems (see Fig. S10 and Fig. S11 of the SM [48]),

analogously to the complex phase shift used in MS theory [6]. By using Im(V) of -32 and -40 meV for Co and Cu adatoms, respectively, the calculated LDOS curves (solid) nicely coincide with dI/dV data. Although the imaginary component is negligible compared to the real part of the potential, it reflects a strong coupling to the bulk states in the form of a large (85–95%) attenuation of the bound-state intensity (~60% for the quantum corral in Fig. S11(b) of the SM [48]), consistent with the black-dot behavior reported for quantum corrals [6]. In Fig. 4(b) we further calculate LDOS for the Cu/Cu(111) system for this complex potential (-0.9–$0.04i$ eV) at different positions spanning from the center of Cu adatom (0) to 50 Å away. The bound-state feature transforms into an edgelike state at/beyond 10 Å away from the adatom, in accordance with the behavior reported for Ag and Cu single adatoms on Ag(111) and Cu(111) substrates [23–25]. The reproduced dI/dV data for single adatoms on metallic substrates assure the suitability of our EBEM/EPWE approach for the modeling of adatom-based nanostructures. Furthermore, the required imaginary potential that account for leakage at adatom position into bulk states reflects the difficulty of bound-state measurements in conductance maps. This is clearly seen in the simulated 2D LDOS [Figs. 4(c) and 4(d)] at the bound-state peak energy (-23 meV) in the Cu/Cu(111) system. While sharp intensity is obtained for real adatom potential [Fig. 4(c)], this is significantly suppressed after the inclusion of the imaginary part [Fig. 4(d)]. Likewise, at the Fermi energy ($E - E_0 = 0.445$ eV), the simulated LDOS maps exhibit standing wave pattern around the adatom which is practically identical for purely real and complex potentials, except at adatom position, where intensity at adatom is hardly defined for imaginary lossy potential. Therefore, the identification of bound-state features in conductance maps, which is required to identify the sign of the scattering potential in quantum corrals [Figs. 1(d) and 1(e)] and adatom-based superlattices [Figs. 3(a) and 3(b)], is experimentally challenging. However, by arranging adatoms into superlattices and probing the scattering states instead, the sign of the confining potentials could be unveiled experimentally as demonstrated in Fig. 2 and Fig. 3. Indeed, a faint dI/dV intensity, similar to Fig. 4(d), at the position of adatoms in hexagonal Ce superlattices with a large periodicity (35 Å) is experimentally measured [39], reassuring their negative potential.

The knowledge of the potential sign here addressed should have large implications on the quantum designer of electronic states with on-demand properties and applications. For instance, the CO molecules which act as positive potential barriers have been used to pioneer electronic band structures with exotic Dirac, Kagome, and flat bands [59–61], while artificial molecular orbitals could be recently emulated by positioning individual cesium adatoms on the surface of a semiconductor substrate [62]. Scatterers in the form of negative potential wells, as well as heterogeneous structures made of combinations of positive and negative potentials, are thus expected to widen the range of novel band structures offered, opening the way towards the formation of complex nanoarchitectures with intriguing electronic properties. Furthermore, the potential sign is expected to also impact the quantum mirage and Kondo scattering by magnetic impurities due to the distinct phase shift at the interior of the corral and the

multiple scattering at the negative/positive walls, whereby the empty focus, in elliptical corrals for instance, could be readily altered [63–65]. Of particular interest is the exploration of nanostructures patterned into heavy metal substrates and surface alloys, where spin-orbit interaction is sufficiently large to split the surface-state dispersion which could induce topological effects/gaps in nanostructures and superlattices [66]. Further computational efforts are thus needed to incorporate these ingredients into the simplified EPWE/EBEM approach and a more quantitative consideration of the coupling to bulk states, here modeled simply through the imaginary component of the potential, is required.

IV. CONCLUSION

In conclusion, we employed the EBEM and EPWE simulation methods to unravel the potential sign in adatom-based quantum corrals and superlattices. For confining finite nanostructures, such as quantum corrals, stadiums, and resonators, the experimental dI/dV spectra acquired at the centers are reproducible using positive or negative adatom potentials, and challenging measurements at/nearby adatom positions are required to determine the potential sign, where bound states should emerge solely for negative adatom potentials. We show that the sign of adatom potential can be unambiguously identified without the quest for challenging bound-state measurements when adatoms are arranged into 2D superlattices, where distinct sign-dependent band structures and density of state scattering features develop. Following these arguments, we reproduce the experimental results of Ce hexagonal superlattices with tunable periodicities confirming the negative potential sign of Ce adatoms. The knowledge of the scattering potential sign here explored is of high fundamental importance for the engineering of superlattices with on-demand electronic structures and related applications.

[1] W. Shockley, On the surface states associated with a periodic potential, Phys. Rev. **56**, 317 (1939).

[2] F. Reinert, G. Nicolay, S. Schmidt, D. Ehm, and S. Hüfner, Direct measurements of the *L*-gap surface states on the (111) face of noble metals by photoelectron spectroscopy, Phys. Rev. B **63**, 115415 (2001).

[3] J. Kliewer, R. Berndt, E. V. Chulkov, V. M. Silkin, P. M. Echenique, and S. Crampin, Dimensionality effects in the lifetime of surface states, Science **288**, 1399 (2000).

[4] Y. Pennec, W. Auwärter, A. Schiffrin, A. Weber-Bargioni, A. Riemann, and J. V. Barth, Supramolecular gratings for tuneable confinement of electrons on metal surfaces, Nat. Nanotechnol. **2**, 99 (2007).

[5] M. F. Crommie, C. P. Lutz, and D. M. Eigler, Confinement of electrons to quantum corrals on a metal surface, Science **262**, 218 (1993).

[6] E. J. Heller, M. F. Crommie, C. P. Lutz, and D. M. Eigler, Scattering and absorption of surface electron waves in quantum corrals, Nature (Lond.) **369**, 464 (1994).

[7] M. F. Crommie, C. P. Lutz, D. M. Eigler, and E. J. Heller, Quantum corrals, Physica D **83**, 98 (1995).

[8] C. R. Moon, L. S. Mattos, B. K. Foster, G. Zeltzer, and H. C. Manoharan, Quantum holographic encoding in a two-dimensional electron gas, Nat. Nanotechnol. **4**, 167 (2009).

[9] M. F. Crommie, C. P. Lutz, and D. M. Eigler, Imaging standing waves in a two-dimensional electron gas, Nature (Lond.) **363**, 524 (1993).

[10] Y. Hasegawa and P. Avouris, Direct observation of standing wave formation at surface steps using scanning tunneling spectroscopy, Phys. Rev. Lett. **71**, 1071 (1993).

[11] J. Li, W.-D. Schneider, S. Crampin, and R. Berndt, Tunnelling spectroscopy of surface state scattering and confinement, Surf. Sci. **422**, 95 (1999).

[12] P. Avouris and I.-W. Lyo, Observation of quantum-size effects at room temperature on metal surfaces with STM, Science **264**, 942 (1994).

[13] L. Bürgi, O. Jeandupeux, A. Hirstein, H. Brune, and K. Kern, Confinement of surface state electrons in Fabry-Pérot resonators, Phys. Rev. Lett. **81**, 5370 (1998).

[14] G. Rodary, D. Sander, H. Liu, H. Zhao, L. Niebergall, V. S. Stepanyuk, P. Bruno, and J. Kirschner, Quantization of the electron wave vector in nanostructures: Counting k-states, Phys. Rev. B **75**, 233412 (2007).

[15] F. G. de Abajo, J. Cordón, M. Corso, F. Schiller, and J. E. Ortega, Lateral engineering of surface states-towards surface-state nanoelectronics, Nanoscale **2**, 717 (2010).

[16] C. Didiot, S. Pons, B. Kierren, Y. Fagot-Revurat, and D. Malterre, Nanopatterning the electronic properties of gold surfaces with self-organized superlattices of metallic nanostructures, Nat. Nanotechnol. **2**, 617 (2007).

[17] R. Cao, X. Zhang, B. Miao, Z. Zhong, L. Sun, B. You, A. Hu, and H. Ding, Self-organized gd atomic superlattice on Ag(111): Scanning tunneling microscopy and kinetic Monte Carlo simulations, Surf. Sci. **610**, 65 (2013).

[18] W. Chen, V. Madhavan, T. Jamneala, and M. F. Crommie, Scanning tunneling microscopy observation of an electronic superlattice at the surface of clean gold, Phys. Rev. Lett. **80**, 1469 (1998).

[19] F. Silly, M. Pivetta, M. Ternes, F. Patthey, J. P. Pelz, and W.-D. Schneider, Creation of an atomic superlattice by immersing metallic adatoms in a two-dimensional electron sea, Phys. Rev. Lett. **92**, 016101 (2004).

[20] Z. M. Abd El-Fattah, M. Matena, M. Corso, F. J. García de Abajo, F. Schiller, and J. E. Ortega, Lifshitz transition across the Ag/Cu(111) superlattice band gap tuned by interface doping, Phys. Rev. Lett. **107**, 066803 (2011).

[21] N. V. Khotkevych-Sanina, Y. A. Kolesnichenko, and J. M. van Ruitenbeek, Fermi surface contours obtained from scanning tunneling microscope images around surface point defects, New J. Phys. **15**, 123013 (2013).

[22] I. Piquero-Zulaica, J. Lobo-Checa, Zakaria M. Abd El-Fattah, J. E. Ortega, F. Klappenberger, W. Auwärter, and J. V. Barth, Engineering quantum states and electronic landscapes through surface molecular nanoarchitectures, Rev. Mod. Phys. **94**, 045008 (2022).

[23] F. E. Olsson, M. Persson, A. G. Borisov, J.-P. Gauyacq, J. Lagoute, and S. Fölsch, Localization of the Cu(111) surface state by single Cu adatoms, Phys. Rev. Lett. **93**, 206803 (2004).

[24] L. Limot, E. Pehlke, J. Kröger, and R. Berndt, Surface-state localization at adatoms, Phys. Rev. Lett. **94**, 036805 (2005).

[25] J. Kröger, L. Limot, H. Jensen, R. Berndt, S. Crampin, and E. Pehlke, Surface state electron dynamics of clean and adsorbate-covered metal surfaces studied with the scanning tunnelling microscope, Prog. Surf. Sci. **80**, 26 (2005).

[26] B. Simon, The bound state of weakly coupled schrödinger operators in one and two dimensions, Ann. Phys. **97**, 279 (1976).

[27] A. A. Aligia and A. M. Lobos, Mirages and many-body effects in quantum corrals, J. Phys.: Condens. Matter **17**, S1095 (2005).

[28] J. Figgins, L. S. Mattos, W. Mar, Y.-T. Chen, H. C. Manoharan, and D. K. Morr, Quantum engineered kondo lattices, Nat. Commun. **10**, 5588 (2019).

[29] V. S. Stepanyuk, L. Niebergall, W. Hergert, and P. Bruno, Ab initio study of mirages and magnetic interactions in quantum corrals, Phys. Rev. Lett. **94**, 187201 (2005).

[30] H. Prüser, P. E. Dargel, M. Bouhassoune, R. G. Ulbrich, T. Pruschke, S. Lounis, and M. Wenderoth, Interplay between the Kondo effect and the Ruderman–Kittel–Kasuya–Yosida interaction, Nat. Commun. **5**, 5417 (2014).

[31] L. Gross, F. Moresco, L. Savio, A. Gourdon, C. Joachim, and K.-H. Rieder, Scattering of surface state electrons at large organic molecules, Phys. Rev. Lett. **93**, 056103 (2004).

[32] J. V. Barth, Molecular architectonic on metal surfaces, Annu. Rev. Phys. Chem. **58**, 375 (2007).

[33] F. Klappenberger, D. Kühne, W. Krenner, I. Silanes, A. Arnau, F. J. García de Abajo, S. Klyatskaya, M. Ruben, and J. V. Barth, Tunable quantum dot arrays formed from self-assembled metal-organic networks, Phys. Rev. Lett. **106**, 026802 (2011).

[34] N. Kepčija, T.-J. Huang, F. Klappenberger, and J. V. Barth, Quantum confinement in self-assembled two-dimensional nanoporous honeycomb networks at close-packed metal surfaces, J. Chem. Phys. **142**, 101931 (2015).

[35] I. Piquero-Zulaica, Z. M. A. El-Fattah, O. Popova, S. Kawai, S. Nowakowska, M. Matena, M. Enache, M. Stöhr, A. Tejeda, A. Taleb, E. Meyer, J. E. Ortega, L. H. Gade, T. A. Jung, and J. Lobo-Checa, Effective determination of surface potential landscapes from metal-organic nanoporous network overlayers, New J. Phys. **21**, 053004 (2019).

[36] I. Piquero-Zulaica, A. Sadeghi, M. Kherelden, M. Hua, J. Liu, G. Kuang, L. Yan, J. E. Ortega, Zakaria M. Abd El-Fattah, B. Azizi, N. Lin, and J. Lobo-Checa, Electron transmission through coordinating atoms embedded in metal-organic nanoporous networks, Phys. Rev. Lett. **123**, 266805 (2019).

[37] I. Piquero-Zulaica, J. Li, Z. M. Abd El-Fattah, L. Solianyk, I. Gallardo, L. Monjas, A. K. H. Hirsch, A. Arnau, J. E. Ortega, M. Stöhr, and J. Lobo-Checa, Surface state tunable energy and mass renormalization from homothetic quantum dot arrays, Nanoscale **11**, 23132 (2019).

[38] M. Ternes, C. Weber, M. Pivetta, F. Patthey, J. P. Pelz, T. Giamarchi, F. Mila, and W.-D. Schneider, Scanning-tunneling spectroscopy of surface-state electrons scattered by a slightly disordered two-dimensional dilute "solid": Ce on Ag(111), Phys. Rev. Lett. **93**, 146805 (2004).

[39] M. Ternes, M. Pivetta, F. Patthey, and W.-D. Schneider, Creation, electronic properties, disorder, and melting of two-dimensional surface-state-mediated adatom superlattices, Prog. Surf. Sci. **85**, 1 (2010).

[40] C. Rong-Xing, Z. Xiao-Pu, M. Bing-Feng, S. Liang, W. Di, Y. Biao, and D. Hai-Feng, From self-assembly to quantum guidinga review of magnetic atomic structures on noble metal surfaces, Chin. Phys. B **23**, 038102 (2014).

[41] Z. M. Abd El-Fattah, M. A. Kher-Elden, I. Piquero-Zulaica, F. J. Garcia de Abajo, and J. E. Ortega, Graphene: Free electron scattering within an inverted honeycomb lattice, Phys. Rev. B **99**, 115443 (2019).

[42] M. Kher-Elden, Z. A. El-Fattah, O. Yassin, and M. El-Okr, Refraction-reflection of electrons at lateral metallic interfaces, Phys. B: Condens. Matter **524**, 127 (2017).

[43] P. A. Knipp and T. L. Reinecke, Boundary-element method for the calculation of electronic states in semiconductor nanostructures, Phys. Rev. B **54**, 1880 (1996).

[44] D. Eigler, Quantum corrals, in *Nanostructures and Quantum Effects* (Springer, Berlin, 1994), pp. 311–314.

[45] M. F. Crommie, C. P. Lutz, D. M. Eigler, and E. J. Heller, Waves on a metal surface and quantum corrals, Surf. Rev. Lett. **02**, 127 (1995).

[46] M. A. Kher-Elden, I. Piquero-Zulaica, K. M. Abd El-Aziz, J. E. Ortega, and Z. M. Abd El-Fattah, Metallic bands in chevron-type polyacenes, RSC Adv. **10**, 33844 (2020).

[47] K. Ali, L. Fernández, M. A. Kherelden, A. A. Makarova, I. Píš, F. Bondino, J. Lawrence, D. G. de Oteyza, D. Y. Usachov, D. V. Vyalikh, F. J. García de Abajo, Z. M. A. El-Fattah, J. E. Ortega, and F. Schiller, Atomically-precise texturing of hexagonal boron nitride nanostripes, Adv. Sc. **8**, 2101455 (2021).

[48] See supplemental material (SM) at http://link.aps.org/supplemental/10.1103/PhysRevB.108.205409 for additional information on the comparative experimental dI/dV data and theoretical electronic density of states calculations performed by EPWE and EBEM for several finite and periodic quantum systems including quantum stadiums, quantum corrals of different sizes, adatom-based quantum resonators, square Fe-based superlattice, Ce-based hexagonal superlattices, individual adatoms and quantum corrals with complex potentials.

[49] J. Deyerling, I. Piquero-Zulaica, M. A. Ashoush, K. Seufert, M. A. Kher-Elden, Z. M. Abd El-Fattah, and W. Auwärter, Formation of an extended quantum dot array driven and auto-protected by an atom-thick *h*-BN layer, ACS Nano **17**, 5448 (2023).

[50] Z. M. Abd El-Fattah, M. Matena, M. Corso, M. Ormaza, J. E. Ortega, and F. Schiller, Modifying the Cu(111) shockley surface state by Au alloying, Phys. Rev. B **86**, 245418 (2012).

[51] S. E. Freeney, S. T. P. Borman, J. W. Harteveld, and I. Swart, Coupling quantum corrals to form artificial molecules, SciPost Phys. **9**, 085 (2020).

[52] S. E. Freeney, M. R. Slot, T. S. Gardenier, I. Swart, and D. Vanmaekelbergh, Electronic quantum materials simulated with artificial model lattices, ACS Nanosci. Au **2**, 198 (2022).

[53] N. N. Negulyaev, V. S. Stepanyuk, L. Niebergall, P. Bruno, W. Hergert, J. Repp, K. H. Rieder, and G. Meyer, Direct evidence for the effect of quantum confinement of surface-state electrons on atomic diffusion, Phys. Rev. Lett. **101**, 226601 (2008).

[54] J. Fernández, M. Moro-Lagares, D. Serrate, and A. A. Aligia, Manipulation of the surface density of states of Ag(111) by

means of resonators: Experiment and theory, Phys. Rev. B **94**, 075408 (2016).

[55] P. Avouris, I.-W. Lyo, and P. Molinas-Mata, STM studies of the interaction of surface state electrons on metals with steps and adsorbates, Chem. Phys. Lett. **240**, 423 (1995).

[56] K. Lau and W. Kohn, Indirect long-range oscillatory interaction between adsorbed atoms, Surf. Sci. **75**, 69 (1978).

[57] P. Hyldgaard and M. Persson, Long-ranged adsorbate-adsorbate interactions mediated by a surface-state band, J. Phys.: Condens. Matter **12**, L13 (2000).

[58] J. Hu, B. Teng, F. Wu, and Y. Fang, Fe nanostructures stabilized by long-range interactions on Cu(111): Kinetic monte carlo simulations, New J. Phys. **10**, 023033 (2008).

[59] K. K. Gomes, W. Mar, W. Ko, F. Guinea, and H. C. Manoharan, Designer dirac fermions and topological phases in molecular graphene, Nature (Lond.) **483**, 306 (2012).

[60] M. R. Slot, T. S. Gardenier, P. H. Jacobse, G. C. Van Miert, S. N. Kempkes, S. J. Zevenhuizen, C. M. Smith, D. Vanmaekelbergh, and I. Swart, Experimental realization and characterization of an electronic lieb lattice, Nat. Phys. **13**, 672 (2017).

[61] T. S. Gardenier, J. J. van den Broeke, J. R. Moes, I. Swart, C. Delerue, M. R. Slot, C. M. Smith, and D. Vanmaekelbergh, p orbital flat band and dirac cone in the electronic honeycomb lattice, ACS Nano **14**, 13638 (2020).

[62] E. Sierda, X. Huang, D. I. Badrtdinov, B. Kiraly, E. J. Knol, G. C. Groenenboom, M. I. Katsnelson, M. Rösner, D. Wegner, and A. A. Khajetoorians, Quantum simulator to emulate lower-dimensional molecular structure, Science **380**, 1048 (2023).

[63] H. Prüser, M. Wenderoth, P. E. Dargel, A. Weismann, R. Peters, T. Pruschke, and R. G. Ulbrich, Long-range Kondo signature of a single magnetic impurity, Nat. Phys. **7**, 203 (2011).

[64] G. A. Fiete, J. S. Hersch, E. J. Heller, H. C. Manoharan, C. P. Lutz, and D. M. Eigler, Scattering theory of Kondo mirages and observation of single Kondo atom phase shift, Phys. Rev. Lett. **86**, 2392 (2001).

[65] G. A. Fiete and E. J. Heller, Colloquium: Theory of quantum corrals and quantum mirages, Rev. Mod. Phys. **75**, 933 (2003).

[66] J. J. van den Broeke, I. Swart, C. M. Smith, and D. Vanmaekelbergh, Effective spin-orbit gaps in the s and p orbital bands of an artificial honeycomb lattice, Phys. Rev. Mater. **5**, 116001 (2021).